Article

Fluorescence Lifetime Imaging of Membrane Lipid Order with a Ratiometric Fluorescent Probe

Vasyl Kilin,[1] Oleksandr Glushonkov,[1] Lucas Herdly,[1] Andrey Klymchenko,[1] Ludovic Richert,[1] and Yves Mely[1,*]
[1]Laboratoire de Biophotonique et Pharmacologie, UMR 7213 CNRS, Faculté de Pharmacie, Université de Strasbourg, Illkirch Cedex, France

ABSTRACT To monitor the lateral segregation of lipids into liquid-ordered (Lo) and -disordered (Ld) phases in lipid membranes, environment-sensitive dyes that partition in both phases but stain them differently have been developed. Of particular interest is the dual-color F2N12S probe, which can discriminate the two phases through the ratio of its two emission bands. These bands are associated with the normal (N*) and tautomer (T*) excited-state species that result from an excited-state intramolecular proton transfer. In this work, we investigated the potency of the time-resolved fluorescence parameters of F2N12S to discriminate lipid phases in model and cell membranes. Both the long and mean lifetime values of the T* form of F2N12S were found to differ by twofold between Ld and Lo phases as a result of the restriction in the relative motions of the two aromatic moieties of F2N12S imposed by the highly packed Lo phase. This differed from the changes in the ratio of the two emission bands between the two phases, which mainly resulted from the decreased hydration of the N* form in the Lo phase. Importantly, the strong difference in lifetimes between the two phases was preserved when cholesterol was added to the Ld phase. The two phases could be imaged with high contrast by fluorescence lifetime imaging microscopy (FLIM) on giant unilamellar vesicles. FLIM images of F2N12S-labeled live HeLa cells confirmed that the plasma membrane was mainly in the Lo-like phase. Furthermore, the two phases were found to be homogeneously distributed all over the plasma membrane, indicating that they are highly mixed at the spatiotemporal resolution of the FLIM setup. Finally, FLIM could also be used to sensitively monitor the change in lipid phase upon cholesterol depletion and apoptosis.

INTRODUCTION

Plasma membrane (PM) bilayers contain a large number of lipid species that differ in their hydrocarbon chain length, saturation, and headgroup (1). A variety of PM biological functions, such as regulation of membrane protein activity, membrane trafficking, and signal transduction, are thought to be related to the lateral segregation of lipids into domains (2–4). Lipid domains enriched in saturated lipids (mainly sphingolipids) and sterols (mainly cholesterol (Chol)) are believed to form a liquid-ordered (Lo)-like phase with strongly packed lipids. These domains may behave as rafts floating on a sea constituted by the loosely packed liquid-disordered (Ld)-like phase enriched in unsaturated phospholipids (2,5,6). However, detection and visualization of these domains is not a simple task (7,8). Various percentages of Lo phase (10–80%) and a rather large range of Lo domain sizes (10–1000 nm) in PMs have been reported depending on the technique used to detect them (9–14).

To noninvasively investigate these domains, investigators have developed fluorescence labels that are selective for a particular phase (15), such as the fluorescently labeled protein cholera toxin-B (CT-B) from *Vibrio cholerae*, which binds rather selectively to the ganglioside GM1 associated with Lo-phase domains, but can induce lipid domains by itself due to its tendency to aggregate (10,16,17). Unfortunately, most molecular membrane probes, notably lipid-like probes, are not suited for staining Lo-phase domains due to their exclusion from the tightly packed Lo phase (3). Nonetheless, as exceptions to this rule, a few saturated lipids that are fluorescently labeled at their headgroups (5,11) and a small number of fluorescent dyes with long alkyl chains, such as LcTMA-DPH (18) and diI-C20 (19), preferentially partition in Lo domains. However, this partition depends on the lipid composition of the Lo domain (20). Molecular rotors such as BODIPY-FL-C_{12}, BODIDY-FL-DHPE, and $DiOC_{18}$ (21) are powerful tools for monitoring microscopic viscosity (22–25) and can also discriminate Lo and Ld phases, but suffer from their preferential partitioning in the Ld phase. Alternatively, lipid domains can be investigated by environment-sensitive probes such as Laurdan (20,26) and its derivatives (27,28), as well as di-4-ANEPPQ (29,30) and NR12S (31). These probes partition in both Lo and Ld phases but change their emission color in response to changes in the lipid phase, which can be detected by ratiometric techniques (26,32). Of particular interest is N-[[4′-N,N-diethylamino-3-hydroxy-6-flavonyl]-methyl]-N-methyl-N-(3-sulfopropyl)-1-dodecanaminium, inner salt (F2N12S), which is highly sensitive to the lipid order of lipid bilayers (33,34). F2N12S is a 3-hydroxyflavone (3HF) probe that exhibits a dual emission as a result of an excited-state intramolecular

Submitted January 13, 2015, and accepted for publication April 3, 2015.
*Correspondence: yves.mely@unistra.fr
Editor: Tobias Baumgart.

0006-3495/15/05/2521/11 $2.00
http://dx.doi.org/10.1016/j.bpj.2015.04.003

proton transfer (ESIPT) reaction generating two different excited-state species (34). Being conjugated to a zwitterion headgroup and a long alkyl chain, the F2N12S fluorophore is selectively anchored at the PM outer leaflet (33), whereas its fluorophore moiety is thought to adopt two slightly different positions and orientations (Fig. 1) (35).

The deepest and more vertical orientation is thought to be associated with a hydrogen (H)-bond-free form that can undergo ESIPT, thus providing the normal (N*) and tautomer (T*) excited-state forms. The more shallow location and tilted orientation is associated with an H-bonded form in which the fluorophore forms an intermolecular H-bond with water. This H-bond is thought to prevent the ESIPT reaction, so only the H-bonded normal form (H-N*) can emit. The emission spectra of the three forms (N*, H-N*, and T*) can be obtained by deconvolution (34,36), which allows one to characterize the polarity of the H-bond-free form through the N*/T* ratio, as well as the hydration parameter through the relative contribution of the H-N* form. In model membranes, F2N12S is highly sensitive to the lipid order and surface charge (33,34). Whereas the Ld-to-Lo transition drastically decreases the hydration parameter, a change in the surface charge mainly affects the polarity parameter. F2N12S was successfully used to monitor changes in the lipid phase of the PM of live cells upon Chol extraction and apoptosis (33). So far, all applications of F2N12S, and notably its imaging in cells, have relied on ratiometric measurements. Although ratiometric imaging is sensitive, it requires a calibration step with model systems of pure phase, as well as a precise alignment of detectors at two different wavelengths (32,37). An alternative is fluorescence lifetime imaging microscopy (FLIM), which registers the fluorescence lifetime values in each pixel of the image independently of the instrumentation used and with no need for a calibration step. Previous studies have shown the advantages of using fluorescence lifetimes to investigate lipid phases in cells (38–40), in particular using Laurdan to estimate the fraction of Lo-like phase in the PM of live cells (41).

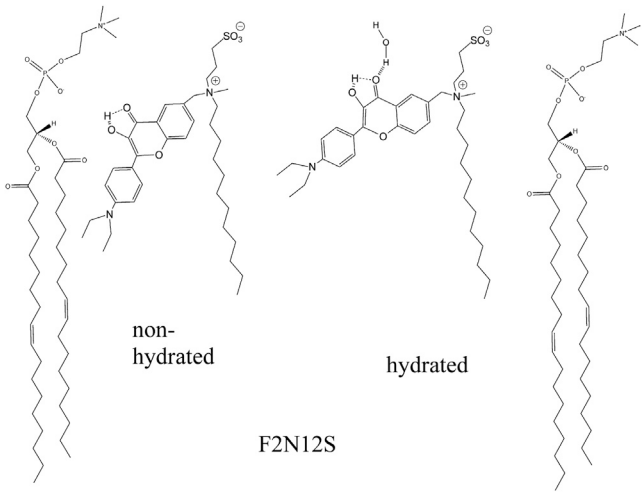

FIGURE 1 Location and orientation of the hydrated and nonhydrated forms of the F2N12S probe in a lipid bilayer.

In this context, our objective in this work was to determine the sensitivity of F2N12S time-resolved fluorescence parameters to the lipid phase and Chol content in large unilamellar vesicles (LUVs) and giant unilamellar vesicles (GUVs), and to validate FLIM as a method for monitoring lipid phases in cells. Our data show that the long and mean lifetimes of the T* band of F2N12S differ by a factor of 2 between the Lo and Ld phases, and thus can be used by FLIM to sensitively and straightforwardly monitor the changes in lipid phase in cells.

MATERIALS AND METHODS

Materials

All chemicals and solvents used in this work were obtained from Sigma-Aldrich. F2N12S was synthesized as previously described (33). The probe was pure according to thin-layer chromatography, ^{1}H-NMR data, absorption, and fluorescence spectra in organic solvents.

Model membranes

LUVs and GUVs were obtained by extrusion and electroformation, respectively (42–44), as described in the Supporting Material.

Cell lines, culture conditions, and treatment

HeLa cells were grown in Dulbecco's modified Eagle's medium (DMEM, high glucose; GIBCO-Invitrogen) supplemented with 10% (v/v) fetal bovine serum (Lonza) and 1% antibiotic solution (penicillin-streptomycin; GIBCO-Invitrogen) in a humidified incubator with 5% CO_2 atmosphere at 37°C.

Chol was depleted with methyl-β-cyclodextrin (MβCD) (Sigma-Aldrich). In short, a stock solution of MβCD in Dulbecco's PBS was prepared at an appropriate concentration, filtered by a Millipore filter (0.22 μm), and added to the cells to a final concentration of 5 mM. Treated cells were kept in the incubator at 37°C for 30 min and then washed with PBS buffer. A stock solution of F2N12S in DMSO was diluted in PBS and added to the cells to a final concentration of 0.1 μM per 10^6 cells (<0.25% DMSO volume), and the cells were incubated for 2 min in the dark at 37°C. To induce apoptosis, the cells were treated with actinomycin D (0.5 μg/mL) for 18 h at 37°C.

In steady-state and time-resolved fluorescence experiments, cells were trypsinized to detach them from the dish surface. The culture medium was first removed from the culture dish and then the cells were washed two times with PBS buffer. Trypsin 10× (Lonza) solution was diluted 10 times with PBS and added to the cells at 37°C for 3 min. The trypsinized cells in solution were then diluted by Hank's balanced salt solution (HBSS), transferred to Falcon tubes, and centrifuged two times at 1500 rpm for 5 min. For staining, an aliquot of probe stock solution in DMSO was added to 0.5 mL of HBSS buffer, and after vortexing, the solution was immediately added to 0.5 mL of the cell suspension (10^6 cells/mL) to obtain a final F2N12S concentration of 0.1 μM (<0.25% DMSO). It should be noted that only freshly prepared solutions of F2N12S in HBSS (<1 min old) should be used for cell staining, because of its slow aggregation in water. The cell suspension was incubated with the probe for 7 min at room temperature in the dark before spectra were recorded or time-resolved fluorescence experiments were performed.

For microscopy experiments, cells were seeded onto a chambered coverglass (IBiDi) at a density of 5×10^4 cells/IBiDi. After 18–24 h, the cells were washed with PBS and then stained by adding a freshly prepared solution of F2N12S in PBS to a final concentration of 0.1 μM per 10^6 cells

(<0.25% DMSO volume), and incubated for 2 min in the dark at room temperature. The cells were then washed again with PBS buffer.

Steady-state and time-resolved fluorescence spectroscopy

Absorption and fluorescence spectra were recorded on a Cary 4000 spectrophotometer (Varian) and a FluoroMax 3.0 (Jobin Yvon, Horiba) spectrofluorometer, respectively. Fluorescence emission spectra were recorded using a 315 nm excitation wavelength at room temperature. All of the spectra were corrected for the fluorescence of the corresponding blank (suspension of cells or lipid vesicles without the probe) and the wavelength dependence of the optical elements in the emission pathway. Deconvolution of F2N12S fluorescence spectra into three bands (N*, H-N*, and T*) was carried out (36) using the PeakFit 4 software as described in the Supporting Material.

We performed single-point time-resolved fluorescence measurements in cuvettes using the time-correlated, single-photon counting (TCSPC) technique with the frequency-tripled output of a Ti-sapphire laser pumped by a Millenia X laser (Tsunami; Spectra Physics) (45). The excitation wavelength was set at 315 nm. The fluorescence decays were collected at the magic angle (54.7°) of the emission polarizer to avoid artifacts due to the vertically polarized excitation beam. Single-photon events were detected with a microchannel plate photomultiplier (R3809-U; Hamamatsu) coupled to a pulse preamplifier (HFAC; Becker & Hickl) and recorded on an SPC-130 board (Becker & Hickl). The instrumental response function was recorded using a polished aluminum reflector, and its full width at half-maximum was ~40 ps. We analyzed the time-resolved decays using the maximum of entropy method (46,47) with Pulse 5 software (Maximum Entropy Data Consultants), which allowed us to resolve fluorescence lifetimes down to ~20 ps. The goodness of the fit was evaluated from the χ^2 values, which ranged from 0.9 to 1.2, and from the plot of the residuals and the autocorrelation function. The mean lifetime was calculated by $\tau_m = \sum \alpha_i \tau_i$, using the lifetimes τ_i associated with positive α_i amplitudes. Decay-associated spectra (DAS) were calculated by : $I_i(\lambda) = a_i\tau_i I(\lambda)/\sum a_i(\lambda)\tau_i$, where $I(\lambda)$ is the steady-state emission spectrum and $a_i(\lambda)$ are the wavelength-dependent amplitudes.

Two-photon FLIM

We performed two-photon fluorescence microscopy at 20°C by using an in-house-built two-photon laser scanning setup based on an Olympus IX70 inverted microscope with an Olympus 60× 1.2NA water immersion objective and two fast galvo mirrors in the descanned fluorescence collection mode (48,49). Two-photon excitation was provided by a titanium-sapphire laser (Tsunami; Spectra Physics) or an Insight DeepSee laser (Spectra Physics). The typical excitation power was ~2.5 mW (λ = 830 nm) at the sample. Photons were detected using an avalanche photodiode (SPCM-AQR-14-FC; Perkin Elmer) coupled to an HQ 585/40 bandpass filter and a single-photon-counting TCSPC module (SPC830; Becker & Hickl) operating in the reversed start-stop mode. Acquisition times were adjusted to achieve 1000 photons per pixel. The minimum fluorescence lifetime detectable with this setup is ~300 ps. FLIM data were analyzed with a binning of one using the SPCImage V4.6 software (Becker & Hickl), which uses an iterative reconvolution method to recover the lifetimes from the fluorescence decays (50). The goodness of the fit was evaluated from the χ^2 values, which ranged from 0.9 to 1.2, and from the plot of the residuals.

RESULTS

LUVs labeled by F2N12S

As the first step in characterizing the dependence of the time-resolved fluorescence parameters on the lipid phase, we investigated the fluorescence intensity decays of F2N12S in LUVs of a controlled lipid composition (Fig. S1). LUVs were chosen as model membranes because they can be easily prepared with any composition. LUVs composed of DOPC lipids were used as models of the Ld phase, and LUVs composed of sphingomyelin (SM) and Chol at a ratio of 2:1 were used as models of the Lo phase. We performed time-resolved fluorescence measurements using the TCSPC technique with a setup that allowed us to record as much as 1 million photons for each decay curve, ensuring excellent statistics. For each type of LUV, decays were recorded at six different emission wavelengths, ranging from 490 to 610 nm (Fig. 2, *A* and *B*; Table S1). For LUVs of both lipid phases, up to five fluorescence lifetimes were recovered, in line with the multiexponential decay reported earlier for this probe in an Ld model membrane (51). As expected for an excited-state reaction such as ESIPT (52), a short lifetime (~30 ps) with a positive amplitude was observed for the N* band, and a corresponding fast-rise component associated with a negative amplitude was observed for the T* form in both phases. This shortest component was almost independent of the phase state. Its value indicated that the ESIPT reaction occurred within 30 ps, so the equilibrium between the N* and T* forms was reached very rapidly in both lipid phases. The values of the intermediate lifetimes (0.1–0.3 ns) and (0.7–1.1 ns) were found to be reasonably close in the two lipid phases (Fig. 2, *A* and *B*). In sharp contrast, the two phases clearly differed with regard to the F2N12S long lifetimes. The Ld phase was characterized by a 2.8 ($\pm$ 0.2) ns component (Fig. 2 *A*), whereas the Lo phase was characterized by a much longer component of 6.0 ($\pm$ 0.2) ns (Fig. 2 *B*). Importantly, the amplitudes of these long lifetimes were observed to strongly increase with the emission wavelength, reaching ~80% at wavelengths $\geq$ 590 nm, so these emission wavelengths were selected for further measurements.

Interestingly, the long lifetime value in the Lo phase (6.0 ns) was very close to that reported for the T* band of a 3HF-based amino acid when it was included in a polystyrene film or when, being part of a peptide, it was stacked with nucleobases in a peptide/oligonucleotide complex (53). For this 3HF-based amino acid, the ~6-ns-long lifetime was clearly related to the restriction of the relative motions of the two aromatic moieties of the 3HF fluorophore, as result of stacking interactions with the polystyrene aromatic rings or the nucleobases, which favored the more planar and emissive 3HF conformation. Therefore, we assumed that the relative motions of the two aromatic rings of the F2N12S fluorophore were also restricted by the highly packed Lo phase, explaining the appearance of the 6.0 ns component as a result of a decrease in the nonradiative deactivation rates. Due to the less constrained packing of lipids in the Ld phase, the restriction in the relative motions of the F2N12S aromatic moieties was certainly less stringent, readily explaining the lower value (2.8 ns) of the long

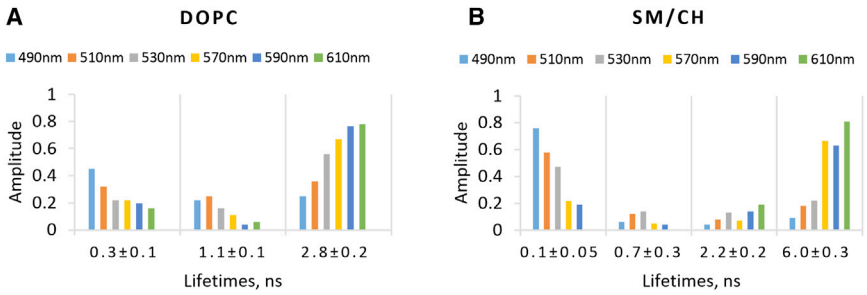

FIGURE 2 Dependence on the emission wavelength of the time-resolved fluorescence parameters of F2N12S in LUVs of Ld and Lo phases. (*A* and *B*) Time-resolved emission decays of F2N12S were recorded in cuvettes for LUVs composed of (*A*) DOPC (Ld phase) and (*B*) SM/Chol (Lo phase). The ~30 ps component describing the ESIPT reaction was omitted in the graph. The emission wavelengths are indicated by the color code. The excitation wavelength was 315 nm. To see this figure in color, go online.

lifetime in this case. Notably, a 2.2 (± 0.1) ns component was also observed in the Lo phase. However, due to its low amplitude (<19%), this 2.2 ns component is expected to only marginally interfere with the determination of the Lo and Ld phases in systems where both phases are present.

As an alternative to the long lifetimes, the values of the mean lifetime τ_m can also be used to discriminate the two phases. These values are especially selective for the T* band at high emission wavelengths. Indeed, we obtained τ_m values of 2.3 (± 0.1) ns and 5.4 (± 0.5) ns for DOPC LUVs and SM/Chol LUVs, respectively, using the decay parameters at 590 and 610 nm (Fig. S2). Thus, both the long and mean lifetime values differ by a factor of 2 between the Lo and Ld phases, and the two phases can be discriminated with high contrast using FLIM.

The strong dependence of the lifetime amplitudes on the wavelength suggests that the different lifetimes may be associated with different excited-state species. As was shown in previous studies (34,36), three emissive species (N*, H-N*, and T*) contribute to the F2N12S emission spectrum. To attribute the lifetime components to these species, we drew the DAS for all lifetime components and compared them with the spectra of the three species obtained by deconvolution of the emission spectra (Fig. 3) (36). Notably, the emission spectra of F2N12S in DOPC and SM/Chol LUVs differed slightly from those reported in our previous studies (34,54), since they were corrected from the wavelength dependence of the optical elements in the emission pathway. A comparison of the deconvoluted spectra of F2N12S in Ld and Lo phases (Fig. 3, *A* and *B*) indicated that the spectra differed mainly by the large contribution of H-N* in the Ld phase. The absence of the H-N* form in the Lo phase could be readily explained by the strong packing and poor hydration of this phase (36,55), which did not favor this hydrated and tilted form.

A comparison of the deconvoluted emission spectra with the DAS for each lifetime component indicates that the emission of F2N12S in SM/Chol LUVs was largely dominated by the 6.0 ns component (Fig. 3 *A*, *green diamonds*). This finding was fully expected for the T* form, where the amplitude and thus the population associated with the 6.0 ns component represented up to 81% (Fig. 2 *B*), and its fractional contribution to the fluorescence intensity calculated by the product of the component by its amplitude divided by the mean lifetime represented up to 92%. The 6.0 ns component also dominated the emission of the N* band, although its population represented less than 20% in this band (Fig. 2 *B*). The strong contribution of this component in the N* emission resulted from the fact that the most populated component (0.1 ns) of the N* form is very poorly fluorescent and thus contributes little to the N* emission (Fig. 3 *A*, *orange disks*). In DOPC LUVs, the emission spectrum of F2N12S was dominated by the emission associated with the 2.8 ns component. This component was particularly dominant in the case of the H-N* and T* forms, as could be seen from the DAS spectra. In contrast, the emission of the N* band was mainly contributed by the 0.3 ns and 1.1 ns components. The short-decay components (0.1–0.3 ns) with high amplitude observed for the N* band in both Ld and Lo phases are likely due to fast photophysical

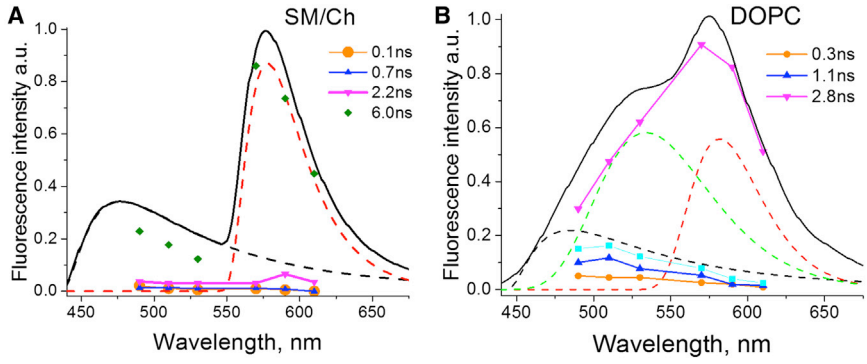

FIGURE 3 (*A* and *B*) DAS overlapped with steady-state spectra and deconvoluted bands of F2N12S in SM/Chol (*A*) and DOPC (*B*) LUVs. Steady-state spectra are represented as solid lines. Deconvoluted spectra of N*, H-N*, and T* bands are drawn with black, green, and red dashed lines, respectively. The DAS for the 0.1 ns, 0.7 ns, and 2.2 ns components in (*A*) and the 0.3 ns, 1.1 ns, and 2.8 ns components in (*B*) are plotted with orange disks, blue triangles, and magenta inverted triangles, respectively. The DAS for the 6 ns component in (*A*) is plotted with green diamonds. The sum of the DAS for 0.3 ns and 1.1 ns components in (*B*) is plotted with cyan squares. To see this figure in color, go online.

processes related to the charge and proton transfer properties of the highly dipolar N* form. On the other hand, the intermediate-decay component (~1 ns) observed for the N* form in DOPC LUVs could be related to the slow relaxation of its lipid environment, as suggested in earlier studies (51,56).

Next, we investigated the dependence of F2N12S time-resolved fluorescence parameters in the Ld phase on the presence of Chol. Chol is a major component of cell membranes, representing up to 50% of their lipid composition (57–59). Its presence in model membranes of the Ld phase was shown to affect the response of Prodan, Laurdan, and di-4-ANEPPDHQ probes (20,26,29,60,61), suggesting that it can affect both membrane order (31,41,54,62) and hydration (36,55). By using Ld LUVs composed of DOPC and increasing Chol fractions, we observed a progressive and substantial decrease of the H-N* band in the F2N12S emission spectra (Fig. 4 *A*). From the deconvoluted spectra, we observed a Chol-induced decrease in the hydration parameter of F2N12S by up to 50% (Fig. 4 *A*, *inset*) at the highest Chol fraction tested (32%), in line with the well-known dehydration effect of Chol in lipid membranes (34,55). However, there was far less dehydration in the Ld phase than in the Lo phase, where the H-N* band was absent.

The time-resolved intensity decays of the DOPC/Chol LUVs were characterized by five lifetime components (Fig. 4 *B*; Table S2). Whereas the long lifetime was identical to that of SM/Chol LUVs (Lo phase), all other lifetimes were similar to those observed in DOPC LUVs (Ld phase). Even at low concentrations, Chol significantly affected the F2N12S environment, as shown by the sharp decrease in the amplitude associated with the 3 ns component, which was mainly to the benefit of the 1 ns component. It can be speculated that a low Chol content in DOPC would induce some disorder in the probe environment, and thus the relative motions between the two aromatic moieties of F2N12S would be less restricted. At higher Chol concentrations, we observed a progressive increase in the amplitude of the 3 ns lifetime, indicating that the probe accumulates in more packed lipid regions, which form as a result of the favorable packing interactions of Chol with lipids. Some of these regions may be rigid enough to allow the 6 ns component to be perceived. However, the amplitude of this 6 ns component ($<-11\%$) is far below that observed in the Lo phase (63%), suggesting that the DOPC/Chol clusters around the F2N12S probe are much more dynamic than the SM/Chol ones. Therefore, the relative amplitudes associated with the 3 and 6 ns components appear to be reliable parameters for discriminating the Lo phase from the Ld phase in both the absence and presence of Chol.

GUVs labeled by F2N12S

LUVs were not appropriate to use for FLIM experiments due to their small size (0.11 μm); therefore, we used GUVs, whose sizes (~10 μm) are perfectly suited for microscopy measurements. In the FLIM technique, a fluorescence decay is recorded at each pixel to extract the fluorescence lifetimes and convert them into a color code. Therefore, the contrast of the obtained images is given by the lifetime values. In contrast to solution measurements, FLIM does not allow recording of more than a few thousand photons per pixel. This results in poor statistics, which precludes analysis of decays with more than one or two lifetime components (50). By monitoring the emission centered at 580 nm, where the contribution of lifetimes of $\leq$2.2 ns are negligible (Fig. 3, *A* and *B*), we should only be able to detect the 2.8 ns component in DOPC GUVs of the Ld phase and the 6 ns component in SM/Chol GUVs of the Lo phase.

In line with our expectations, FLIM measurements (Fig. 5 *A*, *top*) provided rather narrow lifetime distributions centered at 2.7 $\pm$ 0.5 ns for DOPC GUVs and 6.6 $\pm$ 0.6 ns for SM/Chol GUVs (Fig. 5 *B*), which correspond to the long lifetime signatures of the Ld and Lo phases, respectively. Notably, as was found for the ratiometric images, a strong polarization effect could be observed for the Lo phase due to the restricted vertical orientation of F2N12S fluorophore in the lipid bilayer (35,63). Due to the much less constrained environment in the Ld phase, the probe can sample a larger range of orientations, so at each pixel of the GUV bilayer, at least a fraction of the dyes are not perpendicular to the electric field of the laser beam. In GUVs composed of

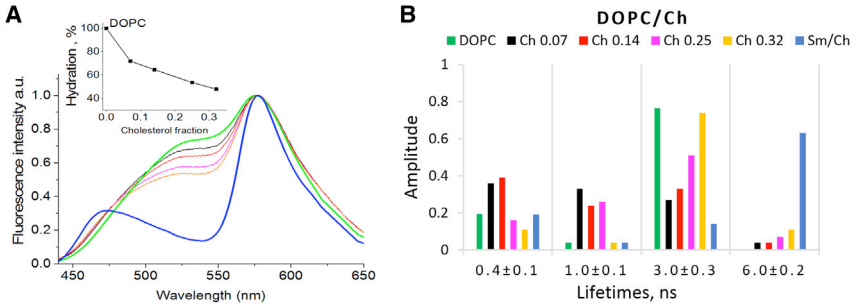

FIGURE 4 Steady-state and time-resolved fluorescence spectroscopy of F2N12S in DOPC/Chol LUVs. (*A*) Steady-state spectra of F2N12S in DOPC/Chol LUVs with increasing fractions of Chol: 0.07 (*black*), 0.14 (*red*), 0.25 (*magenta*), and 0.32 (*orange*). Spectra of F2N12S in DOPC and SM/Chol are in green and blue, respectively. The spectra are normalized at the T* band maximum. (*Inset*) Dependence of the hydration parameter of F2N12S on the Chol fraction in DOPC/Chol LUVs. The probe hydration in DOPC was taken as 100%. (*B*) Time-resolved fluorescence parameters of F2N12S in DOPC/Chol LUVs with increasing Chol fraction. Experiments were performed in cuvettes. Color code as in (*A*). The ~30 ps component describing the ESIPT reaction was omitted in the graph. Emission was recorded at 590 nm. To see this figure in color, go online.

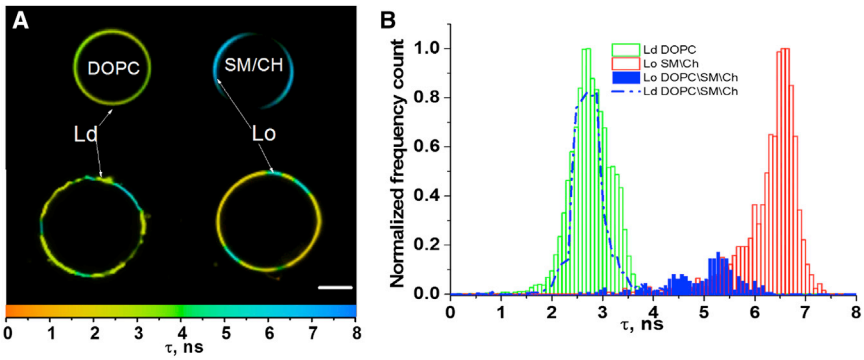

FIGURE 5 FLIM images and lifetime distribution of GUVs of different compositions. (*A*) FLIM images of DOPC (Ld) and SM/Chol (2:1) (Lo) GUVs (*top*). FLIM image of GUVs with SM/DOPC/Chol (1:1:0.7) composition (Lo+Ld) (*bottom*). For each pixel, the lifetime value is coded using the color scale given at the bottom. The scale bar is 10 μm. (*B*) Distribution of lifetime values for the three types of GUVs. To see this figure in color, go online.

DOPC/SM/Chol (1:1:0.7), where the Lo and Ld phases coexist, the two phases could be easily distinguished through their lifetimes, highlighting the ability of the FLIM technique to discriminate the two phases with high contrast. The lifetime of the Ld phase (2.7 $\pm$ 0.5 ns) was found to be very similar to the lifetimes of the DOPC GUVs (Fig. 5 *B*) and the DOPC/Chol (2:1) LUVs (Fig. 4 *B*). In contrast, the lifetime of the Lo phase (5.2 $\pm$ 1 ns) was somewhat shorter than that of the SM/Chol (2:1) GUVs, suggesting that the Lo phase was slightly less ordered in the ternary mixture. This lower-order level probably resulted from the presence of DOPC in the Lo phase of the ternary mixture, which may somewhat reduce the tight packing between SM and Chol in this phase. As a consequence of the clear difference in lifetimes between the two phases, the partition coefficient of F2N12S between the two phases could be estimated. For this purpose, we first measured the size of both domains using ImageJ software (64) on 10 GUVs to estimate the fractional amounts of Lo and Ld phases in these GUVs. We obtained a 75:25 ratio of Ld/Lo phases, in excellent agreement with the 70:30 ratio expected from the phase diagram for GUVs of this composition (65). Next, using SPCimage software, we integrated the number of photons, N_o and N_d, emitted for each of the two phases. We then calculated the partition coefficient of F2N12S between the two phases, P = [Lo]/[Ld], as

$$P = \frac{N_o \phi_d}{N_d \phi_o} \frac{C_d}{C_o}, \quad (1)$$

where ϕ_o (26.5 $\pm$ 3%) and ϕ_d (30 $\pm$ 3%) are the quantum yields of F2N12S in the Lo and Ld phases, respectively, and C_d/C_o is the ratio of the two phases in the GUVs. A p value of 0.17 $\pm$ 0.04 was obtained, indicating a clear preference of F2N12S for the Ld phase.

Cells labeled by F2N12S

Next, we used time-resolved fluorescence approaches to characterize F2N12S-labeled cell membranes. First, we characterized suspensions of intact and Chol-depleted cells using the TCSPC technique. Chol-depleted cells were obtained by incubation with 5 mM MβCD at 37°C for 30 min (31,66). As previously reported for another cell line (U-87 MG) (31), Chol depletion was observed to increase the ratio of short- to long-wavelength bands and red-shift the short-wavelength band (Fig. 6 *A*). The value of the short lifetime associated with the negative amplitude (Table S3) was indistinguishable from the corresponding value in LUVs, indicating that the ESIPT process is only marginally altered by the cell membrane environment or by Chol depletion. Moreover, the amplitudes of the two intermediate lifetimes (0.2 $\pm$ 0.04 and 0.9 $\pm$ 0.2 ns) were low (<10%), so the decays recorded at 590 nm were largely dominated by the two long lifetimes, 3.3 $\pm$ 0.2 ns and 6.9 $\pm$ 0.1 ns, which corresponded to the signatures of the Ld and Lo phases, respectively (Fig. 6 *B*).

In intact cells, the two long lifetimes (3.3 and 6.9 ns) had similar amplitudes (Fig. 6 *B*), giving a mean lifetime of 4.5 $\pm$ 0.5 ns. Both the amplitudes associated with the two long lifetimes and the mean lifetime value are closer to those observed in Lo LUVs as compared with Ld LUVs, confirming that the Lo-like phase may be dominant in cell PMs (34,41,66). Depletion of Chol leads to a redistribution of the amplitudes of the two components (Fig. 6 *B*) with, as expected, a strong decrease of the amplitude of the lifetime associated with the Lo-like phase and thus a strong decrease of the mean lifetime to 2.6 $\pm$ 0.5 ns.

Next, we imaged F2N12S-labeled intact and Chol-depleted HeLa cells using FLIM. We first analyzed the images by employing a single-decay-component model. As previously reported for ratiometric images (31), the FLIM images of intact and Chol-depleted cells labeled with F2N12S showed a remarkable homogeneity in their pseudo-color distribution (Fig. 7 *A*), indicating that no clear phase separation could be perceived. The lifetime distributions were centered at 5.6 $\pm$ 0.9 ns and 3.6 $\pm$ 0.4 ns for intact and Chol-depleted cells, respectively (Fig. 7 *B*). Both lifetimes were intermediate between those observed for the Ld and Lo phases in GUVs (Fig. 5 *B*), suggesting that the two phases may be present in both types of cells. As these two phases could not be discriminated in the FLIM images (Fig. 7 *A*), this suggests that the Lo-like and Ld-like domains are smaller than the ~300 nm resolution

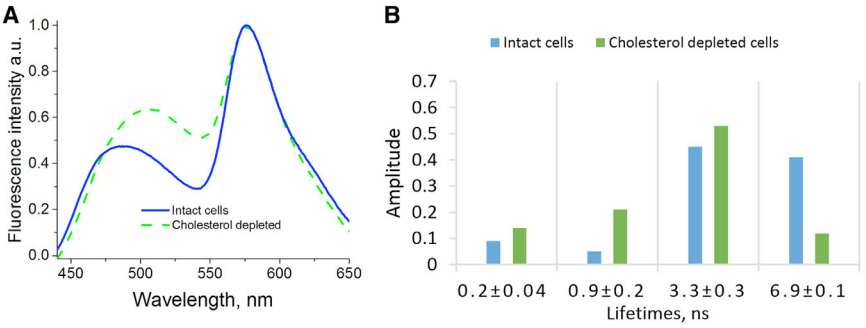

FIGURE 6 (*A* and *B*) Emission spectra (*A*) and time-resolved fluorescence parameters (*B*) of F2N12S-labeled intact (*blue*) and Chol-depleted (*green*) HeLa cells. Time-resolved fluorescence parameters were obtained by TCSPC measurements at 590 nm emission wavelength on cell suspensions in cuvettes. The excitation wavelength was 315 nm. To see this figure in color, go online.

limit of our two-photon excitation microscope and/or that the domains are highly dynamic and thus cannot be resolved in the timescale (approximately seconds) of the FLIM measurements. This is in sharp contrast to the DOPC/SM/Chol GUVs (Fig. 5 *A*), where the separated lipid domains could be easily observed due to their large size and slow dynamics (5,20,35).

As both Lo-like and Ld-like phases are likely present in intact and Chol-depleted cells, we next analyzed the FLIM images using a two-component model to recover the lifetimes and amplitudes associated with the two phases. For intact cells, we obtained $\tau_1 = 3.4 \pm 0.7$ ns and $\tau_2 = 6.4 \pm 0.9$ ns components (Fig. 8, *A* and *B*), which are consistent with the lifetimes of Ld and Lo phases in model systems and the lifetimes recovered by TCSPC measurements on suspensions of the same cells. The two lifetimes recovered by FLIM were found to be homogeneously distributed all over the PM, confirming that the two phases are mixed, at least at the spatiotemporal resolution of the setup. For Chol-depleted HeLa cells, the two lifetime components of F2N12S were $\tau_1 = 2.7 \pm 0.4$ ns and $\tau_2 = 5.4 \pm 0.7$ ns, respectively (Fig. 8, *A* and *B*). The 5.4 ns value for the long lifetime was significantly lower than the 6.9 ns value in TCSPC measurements. This is likely a consequence of there being too few photons in several pixels of the FLIM image, so the analysis could not resolve the two components. In spite of this limitation, it is still obvious from the τ_1 and τ_2 images of Chol-depleted cells (Fig. 8 *A*) that the two phases largely overlap all over the cell PM, suggesting that Chol depletion is not able to unmix the two phases, at least at the spatiotemporal resolution of our FLIM setup.

To further illustrate the potency of our lifetime-based imaging approach, we monitored PM remodeling during apoptosis induced by actinomycin D (0.5 μg/mL; Fig. 9). Using a single-component analysis, we found that apoptotic cells exhibit a lifetime value of 5.1 ± 0.6 ns, which is intermediate between the 5.6 ± 0.9 ns and 3.6 ± 0.4 ns values shown by intact and Chol-depleted cells, respectively. This indicated a decrease in the Lo-like phase (34,62), which probably resulted from the loss of transmembrane asymmetry (67) and the SM hydrolysis into ceramide that occurred during apoptosis (68). A further decreased lifetime value (4.4 ± 0.3 ns) and thus a further decrease in lipid order were observed in vesicles (Fig. 9, *arrows*), which may be attributed to apoptotic blebs (69,70). This decrease in lipid order in apoptotic blebs is fully consistent with the Ld-like phase that Kreder et al. (70) recently described for these blebs by ratiometric imaging using Nile-red based probes.

DISCUSSION

In this work, we investigated the potency of time-resolved fluorescence techniques to discriminate lipid phases in model and cell membranes, using the ratiometric membrane probe F2N12S. Despite the complex multiexponential decay of F2N12S (51), we found that the Lo phase could be discriminated from the Ld phase with high contrast, by the values of its long and mean fluorescence lifetimes. The best sensitivity was observed at the red edge of the F2N12S emission spectrum, where the T* form is dominant. The twofold higher values of the F2N12S long and mean lifetimes in the Lo phase as compared with the Ld

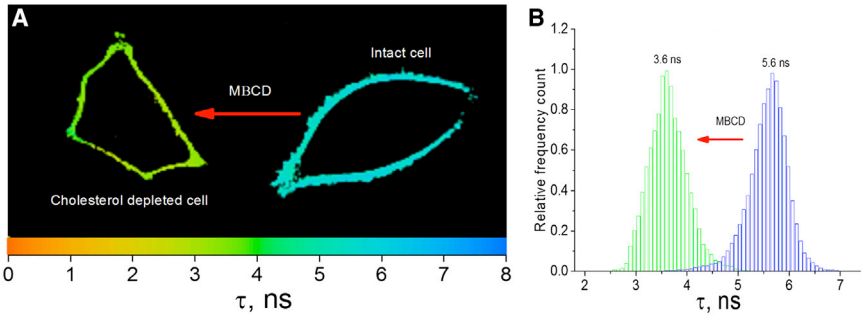

FIGURE 7 FLIM images and lifetime distribution of intact and Chol-depleted HeLa cells, analyzed by a single decay component model. (*A*) FLIM images of Chol-depleted (*left*) and intact (*right*) HeLa cells. The pixel colors describe the lifetime values according to the color scale on the *X* axis. (*B*) Lifetime distribution for intact (*blue*) and Chol-depleted (*green*) cells. The distributions were obtained from measurements on 20 cells. Two-photon excitation was at 830 nm. To see this figure in color, go online.

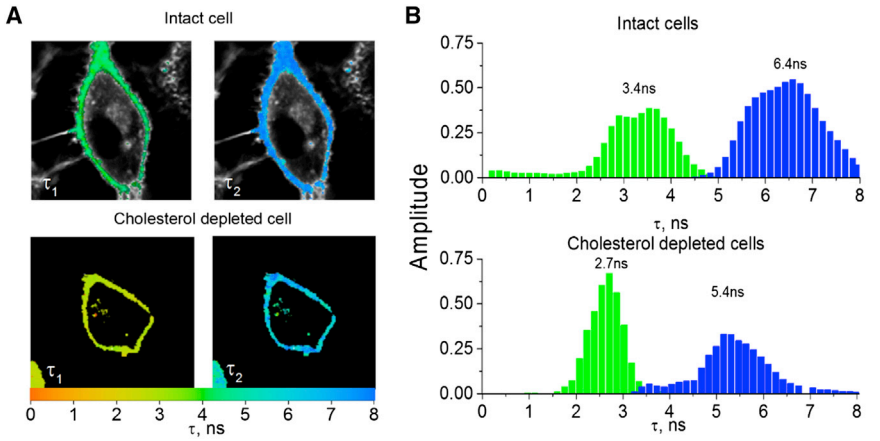

FIGURE 8 FLIM images of F2N12S-labeled intact and Chol-depleted HeLa cells, analyzed by a two-component model. (*A*) FLIM images were recorded as in Fig. 7 and analyzed with a two-component ($\tau1$ and $\tau2$) model. The colors of the pixels describe the values of the $\tau1$ (*left panels*) and $\tau2$ (*right panels*) components according to the color scale on the *X* axis. (*B*) Distribution of the amplitudes associated with the $\tau1$ (*green*) and $\tau2$ (*blue*) components for intact (*top panel*) and Chol-depleted (*bottom panel*) cells. The histograms resulted from measurements on 20 cells. To see this figure in color, go online.

phase were attributed to the restriction in the relative motions of the two aromatic moieties of F2N12S imposed by the highly packed Lo phase, which favored the more planar and more emissive conformation of the 3HF fluorophore (53). Addition of Chol to DOPC LUVs was also found to induce the appearance of the ~6 ns lifetime component, which is characteristic of the Lo phase, but only at low amplitude. This is likely related to the inability of Chol to induce in the Ld phase the strong packing of lipids that characterizes the Lo phase and efficiently restricts the relative motions of the two aromatic moieties of F2N12S. Therefore, the lifetime signatures of the Ld and Lo phases (~3 ns and ~6 ns, respectively) appear to be sensitive tools for distinguishing the two phases even in the presence of Chol. This was confirmed by FLIM images of SM/DOPC/Chol GUVs, where the large and stable Ld and Lo phases could be easily discriminated by their lifetime signatures, although Chol was likely distributed in both phases (Fig. 5). The capacity to distinguish between the Lo and Ld phases in Chol-containing lipid compositions is an important advantage of F2N12S over a number of other environment-sensitive probes, such as Laurdan, in which case the presence of Chol in the Ld phase decreases the contrast with respect to the Lo phase (71).

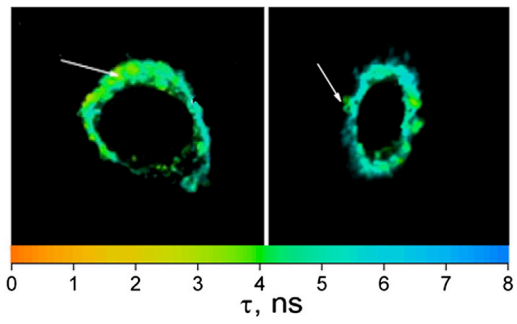

FIGURE 9 FLIM images of apoptotic HeLa cells analyzed by a single-decay-component model. The pixel colors describe the lifetime values according to the color scale on the *X* axis. The arrows show vesicles that can be assigned to blebs. The lifetime values of the blebs suggest that they exhibit an Ld-like phase. To see this figure in color, go online.

The contrast in lifetimes between the two phases observed with F2N12S was found to be significantly higher than that observed for various fluorescence-labeled phospholipids, such as BODIPY-PC (72), Rhod-DOPE (73), and C6-NBD-PC (38,74). Although the last compound was also quite sensitive, showing a 70% difference in lifetime values between the two phases, it provided a much smaller change (<10%) in response to Chol depletion as compared with F2N12S (~60%) and suffered also from low photostability (38). F2N12S also showed improved sensitivity compared with perylene monoimide derivatives, which are highly bright and photostable, but undergo a smaller change (35%) in their lifetime between Ld and Lo phases and suffer from their tendency to aggregate (39).

The ~2-fold variation in F2N12S lifetimes between Lo and Ld phases is comparable to the variation in the general polarization or the two-band ratio values observed with Laurdan (41), PY series (40), di-4-ANEPPDHQ (30,38,39), and NR12S (31) probes. However, since fluorescence lifetimes are absolute parameters that are independent of the instrumentation used, no calibration is required, in contrast to ratiometric methods, which are based on intensity measurements (26,31,33,75). Moreover, a key feature of F2N12S is its capacity to bind specifically to the outer leaflet of the PM. This is of crucial importance for two reasons. First, since the PM is asymmetric, with the outer leaflet being highly enriched in SM, Lo domains are particularly important in this leaflet. As a result, the information revealed by F2N12S at the PM is not complicated by staining of the inner leaflet. Second, since F2N12S is anchored at the outer leaflet, it does not diffuse rapidly inside the cell to stain the inner lipid membranes. As a result, the contrast of the FLIM images at the PM is not decreased by photons coming from inner compartments close to the PM. A frequently used alternative to FLIM imaging is the phasor plot approach (76,77). Although this method is also based on fluorescence decays, it requires a calibration step with

compounds exhibiting single lifetimes (41,77). The contrast obtained by F2N12S lifetime analysis is also comparable to that reported for the ratio of its two emission bands (34). More importantly, the contrast offered by the lifetime analysis and the intensity ratio differs according to its origin. Whereas ratiometric measurements are mainly sensitive to F2N12S hydration, fluorescence lifetimes mainly reflect the local dynamics of F2N12S in its lipid environment. The F2N12S fluorescence lifetimes measured at 580 nm are poorly sensitive to hydration or solvent relaxation effects because the T* form, in contrast to the N* form, exhibits low dipole moment in its excited state (78–80). Therefore, FLIM and ratiometric imaging with F2N12S are two complementary approaches for studying lipid membranes. Remarkably, when the Lo and Ld phases are compared, these two parameters correlate because the increase in the membrane rigidity (observed by lifetimes) is a result of tight packing in the Lo phase, which expels water from the membrane (observed by the ratio).

Whereas the time-resolved fluorescence parameters of F2N12S in the Ld phase were only moderately sensitive to Chol, it nevertheless appears that DOPC LUVs, which are frequently used as an Ld phase standard (34,41), do not appropriately mimic the Chol-rich Ld-like phase in cell membranes. It is likely that other lipids (in particular, partially unsaturated ones such as POPC) may also affect the local dynamics of F2N12S, making it difficult to find the appropriate lipid composition that will faithfully mimic the behavior of F2N12S in the Ld-like phase of cell membranes. The same conclusion likely applies also for the Lo phase. Further complication arises from the fact that, to our knowledge, the exact lipid composition of both phases in cell membranes is still not known. In these conditions, it appears to be very difficult to use this kind of tool to accurately determine the phase composition in cell membranes. Whereas an accurate quantitative determination of the two phases appears unrealistic, the large difference in the lifetimes of the two phases allowed us to reveal by FLIM that both Lo-like and Ld-like phases were distributed all over the PM of intact and Chol-depleted live cells. No separation of the two phases could be observed, suggesting that the two phases are mixed over the PM in our measurement conditions. This suggests that the two phases are highly dynamic on the timescale of the measurements (seconds) and/or that one or both phases show subdiffraction sizes ($<$250 nm), supporting the notion that lipid domains in cell membranes may be small and highly dynamic (81,82). In line with previous reports (31,34,41,54,62,66,83), the Lo-like phase was clearly dominant in live cells, whereas Chol depletion or apoptosis was found to increase the Ld-like phase. Thus, our data on the coexistence of the two phases and the prevalence of the Lo-like phase in intact cells are in line with a previous model suggesting that the PM may be constituted by a continuous Lo-like phase filled with Ld-like holes or, alternatively, by a continuous Ld-like phase containing a large number of Lo domains that cannot be spatially resolved (41).

Taken together, our data indicate that the use of F2N12S with lifetime-based approaches allows one to distinguish Lo from Ld phases with high contrast. We successfully used this technique to monitor membrane remodeling in F2N12S-labeled cells during various physiological processes, such as apoptosis. Further characterization of the membrane phases will require techniques with either faster acquisition rates than FLIM, such as fluorescence lifetime-transient scanning (FLITS, with a millisecond acquisition time (50)), or higher spatial resolution, such as single-particle tracking (82) and stimulated emission depletion-fluorescence correlation spectroscopy (STED-FCS) (81,84). Experiments using these techniques are currently being conducted on F2N12S-labeled cells.

SUPPORTING MATERIAL

Supporting Materials and Methods, two figures, and three tables are available at http://www.biophysj.org/biophysj/supplemental/S0006-3495(15)00349-5.

AUTHOR CONTRIBUTIONS

V.K., O.G., and L.H. performed research and analyzed the data. Y.M. designed research. V.K., A.K., L.R., and Y.M. wrote the article.

ACKNOWLEDGMENTS

We thank Nicolas Humbert, Ny Hanitra Andriamora, and Sule Oncul for technical assistance.

This work was supported by the University of Strasbourg and CNRS.

REFERENCES

1. Mouritsen, O. G. 2011. Lipidology and lipidomics—quo vadis? A new era for the physical chemistry of lipids. *Phys. Chem. Chem. Phys.* 13:19195–19205.
2. Brown, D. A., and J. K. Rose. 1992. Sorting of GPI-anchored proteins to glycolipid-enriched membrane subdomains during transport to the apical cell surface. *Cell.* 68:533–544.
3. van Meer, G., and K. Simons. 1988. Lipid polarity and sorting in epithelial cells. *J. Cell. Biochem.* 36:51–58.
4. Simons, K., and D. Toomre. 2000. Lipid rafts and signal transduction. *Nat. Rev. Mol. Cell Biol.* 1:31–39.
5. Dietrich, C., L. A. Bagatolli, …, E. Gratton. 2001. Lipid rafts reconstituted in model membranes. *Biophys. J.* 80:1417–1428.
6. Veatch, S. L., and S. L. Keller. 2002. Organization in lipid membranes containing cholesterol. *Phys. Rev. Lett.* 89:268101.
7. Lommerse, P. H., H. P. Spaink, and T. Schmidt. 2004. In vivo plasma membrane organization: results of biophysical approaches. *Biochim. Biophys. Acta.* 1664:119–131.
8. Pike, L. J. 2006. Rafts defined: a report on the Keystone Symposium on Lipid Rafts and Cell Function. *J. Lipid Res.* 47:1597–1598.
9. Pralle, A., P. Keller, …, J. K. H. Hörber. 2000. Sphingolipid-cholesterol rafts diffuse as small entities in the plasma membrane of mammalian cells. *J. Cell Biol.* 148:997–1008.

10. Dietrich, C., B. Yang, …, K. Jacobson. 2002. Relationship of lipid rafts to transient confinement zones detected by single particle tracking. *Biophys. J.* 82:274–284.

11. Schütz, G. J., G. Kada, …, H. Schindler. 2000. Properties of lipid microdomains in a muscle cell membrane visualized by single molecule microscopy. *EMBO J.* 19:892–901.

12. Lenne, P. F., L. Wawrezinieck, …, D. Marguet. 2006. Dynamic molecular confinement in the plasma membrane by microdomains and the cytoskeleton meshwork. *EMBO J.* 25:3245–3256.

13. Sharma, P., R. Varma, …, S. Mayor. 2004. Nanoscale organization of multiple GPI-anchored proteins in living cell membranes. *Cell.* 116:577–589.

14. Swamy, M. J., L. Ciani, …, J. H. Freed. 2006. Coexisting domains in the plasma membranes of live cells characterized by spin-label ESR spectroscopy. *Biophys. J.* 90:4452–4465.

15. Demchenko, A. P., Y. Mély, …, A. S. Klymchenko. 2009. Monitoring biophysical properties of lipid membranes by environment-sensitive fluorescent probes. *Biophys. J.* 96:3461–3470.

16. Janes, P. W., S. C. Ley, and A. I. Magee. 1999. Aggregation of lipid rafts accompanies signaling via the T cell antigen receptor. *J. Cell Biol.* 147:447–461.

17. Kenworthy, A. K., N. Petranova, and M. Edidin. 2000. High-resolution FRET microscopy of cholera toxin B-subunit and GPI-anchored proteins in cell plasma membranes. *Mol. Biol. Cell.* 11:1645–1655.

18. Xu, X., R. Bittman, …, E. London. 2001. Effect of the structure of natural sterols and sphingolipids on the formation of ordered sphingolipid/sterol domains (rafts). Comparison of cholesterol to plant, fungal, and disease-associated sterols and comparison of sphingomyelin, cerebrosides, and ceramide. *J. Biol. Chem.* 276:33540–33546.

19. Korlach, J., P. Schwille, …, G. W. Feigenson. 1999. Characterization of lipid bilayer phases by confocal microscopy and fluorescence correlation spectroscopy. *Proc. Natl. Acad. Sci. USA.* 96:8461–8466.

20. Bagatolli, L. A. 2006. To see or not to see: lateral organization of biological membranes and fluorescence microscopy. *Biochim. Biophys. Acta.* 1758:1541–1556.

21. Wu, Y., M. Stefl, …, M. K. Kuimova. 2013. Molecular rheometry: direct determination of viscosity in Lo and Ld lipid phases via fluorescence lifetime imaging. *Phys. Chem. Chem. Phys.* 15:14986–14993.

22. Kuimova, M. K., G. Yahioglu, …, K. Suhling. 2008. Molecular rotor measures viscosity of live cells via fluorescence lifetime imaging. *J. Am. Chem. Soc.* 130:6672–6673.

23. Levitt, J. A., M. K. Kuimova, …, D. Phillips. 2009. Membrane-bound molecular rotors measure viscosity in live cells via fluorescence lifetime imaging. *J. Phys. Chem. C.* 113:11634–11642.

24. Kuimova, M. K., S. W. Botchway, …, P. R. Ogilby. 2009. Imaging intracellular viscosity of a single cell during photoinduced cell death. *Nat. Chem.* 1:69–73.

25. Haidekker, M. A., and E. A. Theodorakis. 2007. Molecular rotors—fluorescent biosensors for viscosity and flow. *Org. Biomol. Chem.* 5:1669–1678.

26. Parasassi, T., E. Gratton, …, M. Levi. 1997. Two-photon fluorescence microscopy of laurdan generalized polarization domains in model and natural membranes. *Biophys. J.* 72:2413–2429.

27. Kim, H. M., H.-J. Choo, …, B. R. Cho. 2007. A two-photon fluorescent probe for lipid raft imaging: C-laurdan. *ChemBioChem.* 8:553–559.

28. Kim, H. M., B. H. Jeong, …, B. R. Cho. 2008. Two-photon fluorescent turn-on probe for lipid rafts in live cell and tissue. *J. Am. Chem. Soc.* 130:4246–4247.

29. Jin, L., A. C. Millard, …, L. M. Loew. 2005. Cholesterol-enriched lipid domains can be visualized by di-4-ANEPPDHQ with linear and nonlinear optics. *Biophys. J.* 89:L04–L06.

30. Owen, D. M., P. M. Lanigan, …, A. I. Magee. 2006. Fluorescence lifetime imaging provides enhanced contrast when imaging the phase-sensitive dye di-4-ANEPPDHQ in model membranes and live cells. *Biophys. J.* 90:L80–L82.

31. Kucherak, O. A., S. Oncul, …, A. S. Klymchenko. 2010. Switchable nile red-based probe for cholesterol and lipid order at the outer leaflet of biomembranes. *J. Am. Chem. Soc.* 132:4907–4916.

32. Krasnowska, E. K., E. Gratton, and T. Parasassi. 1998. Prodan as a membrane surface fluorescence probe: partitioning between water and phospholipid phases. *Biophys. J.* 74:1984–1993.

33. Shynkar, V. V., A. S. Klymchenko, …, Y. Mely. 2007. Fluorescent biomembrane probe for ratiometric detection of apoptosis. *J. Am. Chem. Soc.* 129:2187–2193.

34. Oncul, S., A. S. Klymchenko, …, Y. Mély. 2010. Liquid ordered phase in cell membranes evidenced by a hydration-sensitive probe: effects of cholesterol depletion and apoptosis. *Biochim. Biophys. Acta.* 1798:1436–1443.

35. Klymchenko, A. S., S. Oncul, …, Y. Mély. 2009. Visualization of lipid domains in giant unilamellar vesicles using an environment-sensitive membrane probe based on 3-hydroxyflavone. *Biochim. Biophys. Acta.* 1788:495–499.

36. M'Baye, G., Y. Mély, …, A. S. Klymchenko. 2008. Liquid ordered and gel phases of lipid bilayers: fluorescent probes reveal close fluidity but different hydration. *Biophys. J.* 95:1217–1225.

37. Parasassi, T., G. De Stasio, …, E. Gratton. 1990. Phase fluctuation in phospholipid membranes revealed by Laurdan fluorescence. *Biophys. J.* 57:1179–1186.

38. Stöckl, M. T., and A. Herrmann. 2010. Detection of lipid domains in model and cell membranes by fluorescence lifetime imaging microscopy. *Biochim. Biophys. Acta.* 1798:1444–1456.

39. Margineanu, A., J. Hotta, …, J. Hofkens. 2007. Visualization of membrane rafts using a perylene monoimide derivative and fluorescence lifetime imaging. *Biophys. J.* 93:2877–2891.

40. Kwiatek, J. M., D. M. Owen, …, K. Gaus. 2013. Characterization of a new series of fluorescent probes for imaging membrane order. *PLoS ONE.* 8:e52960.

41. Owen, D. M., D. J. Williamson, …, K. Gaus. 2012. Sub-resolution lipid domains exist in the plasma membrane and regulate protein diffusion and distribution. *Nat. Commun.* 3:1256.

42. Angelova, M. I., and D. S. Dimitrov. 1986. Liposome electroformation. *Faraday Discuss.* 81:303–311.

43. Fidorra, M., L. Duelund, …, L. A. Bagatolli. 2006. Absence of fluid-ordered/fluid-disordered phase coexistence in ceramide/POPC mixtures containing cholesterol. *Biophys. J.* 90:4437–4451.

44. Kahya, N., D. Scherfeld, …, P. Schwille. 2003. Probing lipid mobility of raft-exhibiting model membranes by fluorescence correlation spectroscopy. *J. Biol. Chem.* 278:28109–28115.

45. Godet, J., N. Ramalanjaona, …, Y. Mély. 2011. Specific implications of the HIV-1 nucleocapsid zinc fingers in the annealing of the primer binding site complementary sequences during the obligatory plus strand transfer. *Nucleic Acids Res.* 39:6633–6645.

46. Livesey, A. K., and J. C. Brochon. 1987. Analyzing the distribution of decay constants in pulse-fluorimetry using the maximum entropy method. *Biophys. J.* 52:693–706.

47. Brochon, J. C. 1994. Maximum entropy method of data analysis in time-resolved spectroscopy. *Methods Enzymol.* 240:262–311.

48. Clamme, J. P., J. Azoulay, and Y. Mély. 2003. Monitoring of the formation and dissociation of polyethylenimine/DNA complexes by two photon fluorescence correlation spectroscopy. *Biophys. J.* 84:1960–1968.

49. Azoulay, J., J. P. Clamme, …, Y. Mély. 2003. Destabilization of the HIV-1 complementary sequence of TAR by the nucleocapsid protein through activation of conformational fluctuations. *J. Mol. Biol.* 326:691–700.

50. Becker, W., V. Shcheslavkiy, …, I. Slutsky. 2014. Spatially resolved recording of transient fluorescence-lifetime effects by line-scanning TCSPC. *Microsc. Res. Tech.* 77:216–224.

51. Das, R., A. S. Klymchenko, …, Y. Mély. 2008. Excited state proton transfer and solvent relaxation of a 3-hydroxyflavone probe in lipid bilayers. *J. Phys. Chem. B.* 112:11929–11935.

52. Shynkar, V. V., Y. Mely, …, A. P. Demchenko. 2003. Picosecond time-resolved fluorescence studies are consistent with reversible excited-state intramolecular proton transfer in 4′-(dialkylaminoe)-3-hydroxyflavones. *J. Phys. Chem. A.* 107:9522–9529.

53. Sholokh, M., O. M. Zamotaiev, …, Y. Mély. 2015. Fluorescent amino acid undergoing excited state intramolecular proton transfer for site-specific probing and imaging of peptide interactions. *J. Phys. Chem. B.* 119:2585–2595.

54. Kilin, V., Z. Darwich, …, Y. Mely. 2013. Two photon fluorescence imaging of lipid membrane domains and potentials using advanced fluorescent probes. *Proc. SPIE.* 8588:13.

55. Parasassi, T., M. Di Stefano, …, E. Gratton. 1994. Cholesterol modifies water concentration and dynamics in phospholipid bilayers: a fluorescence study using Laurdan probe. *Biophys. J.* 66:763–768.

56. Kułakowska, A., P. Jurkiewicz, …, M. Hof. 2010. Fluorescence lifetime tuning—a novel approach to study flip-flop kinetics in supported phospholipid bilayers. *J. Fluoresc.* 20:563–569.

57. Chen, L., Z. Yu, and P. J. Quinn. 2007. The partition of cholesterol between ordered and fluid bilayers of phosphatidylcholine: a synchrotron X-ray diffraction study. *Biochim. Biophys. Acta.* 1768:2873–2881.

58. Huang, J., J. T. Buboltz, and G. W. Feigenson. 1999. Maximum solubility of cholesterol in phosphatidylcholine and phosphatidylethanolamine bilayers. *Biochim. Biophys. Acta.* 1417:89–100.

59. Bloch, K. E. 1979. Speculations on the evolution of sterol structure and function. *CRC Crit. Rev. Biochem.* 7:1–5.

60. Gaus, K., E. Gratton, …, W. Jessup. 2003. Visualizing lipid structure and raft domains in living cells with two-photon microscopy. *Proc. Natl. Acad. Sci. USA.* 100:15554–15559.

61. Massey, J. B. 1998. Effect of cholesteryl hemisuccinate on the interfacial properties of phosphatidylcholine bilayers. *Biochim. Biophys. Acta.* 1415:193–204.

62. Darwich, Z., A. S. Klymchenko, O. A. Kucherak, L. Richert, and Y. Mely. 2012. Detection of apoptosis through the lipid order of the outer plasma membrane leaflet. *Biochim. Biophys. Acta.* 1818:3048–3054.

63. Barucha-Kraszewska, J., S. Kraszewski, …, M. Hof. 2010. Numerical studies of the membrane fluorescent dyes dynamics in ground and excited states. *Biochim. Biophys. Acta.* 1798:1724–1734.

64. Schneider, C. A., W. S. Rasband, and K. W. Eliceiri. 2012. NIH Image to ImageJ: 25 years of image analysis. *Nat. Methods.* 9:671–675.

65. Bezlyepkina, N., R. S. Gracià, …, R. Dimova. 2013. Phase diagram and tie-line determination for the ternary mixture DOPC/eSM/cholesterol. *Biophys. J.* 104:1456–1464.

66. Hao, M., S. Mukherjee, and F. R. Maxfield. 2001. Cholesterol depletion induces large scale domain segregation in living cell membranes. *Proc. Natl. Acad. Sci. USA.* 98:13072–13077.

67. Zwaal, R. F., and A. J. Schroit. 1997. Pathophysiologic implications of membrane phospholipid asymmetry in blood cells. *Blood.* 89:1121–1132.

68. Tepper, A. D., P. Ruurs, …, W. J. van Blitterswijk. 2000. Sphingomyelin hydrolysis to ceramide during the execution phase of apoptosis results from phospholipid scrambling and alters cell-surface morphology. *J. Cell Biol.* 150:155–164.

69. Charras, G. T., M. Coughlin, …, L. Mahadevan. 2008. Life and times of a cellular bleb. *Biophys. J.* 94:1836–1853.

70. Kreder, R., K. A. Pyrshev, …, A. S. Klymchenko. 2015. Solvatochromic Nile Red probes with FRET quencher reveal lipid order heterogeneity in living and apoptotic cells. *ACS Chem. Biol.* Published online March 6: 2015. http://dx.doi.org/10.1021/cb500922m.

71. Parasassi, T., M. Di Stefano, …, E. Gratton. 1994. Influence of cholesterol on phospholipid bilayers phase domains as detected by Laurdan fluorescence. *Biophys. J.* 66:120–132.

72. Ariola, F. S., D. J. Mudaliar, …, A. A. Heikal. 2006. Dynamics imaging of lipid phases and lipid-marker interactions in model biomembranes. *Phys. Chem. Chem. Phys.* 8:4517–4529.

73. de Almeida, R. F., J. Borst, …, A. J. Visser. 2007. Complexity of lipid domains and rafts in giant unilamellar vesicles revealed by combining imaging and microscopic and macroscopic time-resolved fluorescence. *Biophys. J.* 93:539–553.

74. Stöckl, M., A. P. Plazzo, …, A. Herrmann. 2008. Detection of lipid domains in model and cell membranes by fluorescence lifetime imaging microscopy of fluorescent lipid analogues. *J. Biol. Chem.* 283:30828–30837.

75. Balogh, G., G. Maulucci, …, L. Vígh. 2011. Heat stress causes spatially-distinct membrane re-modelling in K562 leukemia cells. *PLoS ONE.* 6:e21182.

76. Jameson, D. M., E. Gratton, and R. D. Hall. 1984. The measurement and analysis of heterogeneous emissions by multifrequency phase and modulation fluorometry. *Applied Spec. Rev.* 20:55–106.

77. Digman, M. A., V. R. Caiolfa, …, E. Gratton. 2008. The phasor approach to fluorescence lifetime imaging analysis. *Biophys. J.* 94:L14–L16.

78. Klymchenko, A. S., and A. P. Demchenko. 2002. Electrochromic modulation of excited-state intramolecular proton transfer: the new principle in design of fluorescence sensors. *J. Am. Chem. Soc.* 124:12372–12379.

79. Kenfack, C. A., A. S. Klymchenko, …, Y. Mély. 2012. Ab initio study of the solvent H-bonding effect on ESIPT reaction and electronic transitions of 3-hydroxychromone derivatives. *Phys. Chem. Chem. Phys.* 14:8910–8918.

80. Demchenko, A. P., K. C. Tang, and P. T. Chou. 2013. Excited-state proton coupled charge transfer modulated by molecular structure and media polarization. *Chem. Soc. Rev.* 42:1379–1408.

81. Eggeling, C., C. Ringemann, …, S. W. Hell. 2009. Direct observation of the nanoscale dynamics of membrane lipids in a living cell. *Nature.* 457:1159–1162.

82. Sahl, S. J., M. Leutenegger, …, C. Eggeling. 2010. Fast molecular tracking maps nanoscale dynamics of plasma membrane lipids. *Proc. Natl. Acad. Sci. USA.* 107:6829–6834.

83. Darwich, Z., O. A. Kucherak, …, A. S. Klymchenko. 2013. Rational design of fluorescent membrane probes for apoptosis based on 3-hydroxyflavone. *Methods Appl. Fluoresc.* 1:025002.

84. Honigmann, A., V. Mueller, …, C. Eggeling. 2014. Scanning STED-FCS reveals spatiotemporal heterogeneity of lipid interaction in the plasma membrane of living cells. *Nat. Commun.* 5:5412.